130 HIGH-RESOLUTION ENSEMBLE EXPERIMENTS FOR THE TSUKUBA CITY SUPERCELL TORNADO IN JAPAN ON 6 MAY 2012

Sho Yokota*[1], Hiromu Seko[1,2], Masaru Kunii[1], Hiroshi Yamauchi[3], and Hiroshi Niino[4]
[1]Meteorological Research Institute, Tsukuba, Japan
[2]Japan Agency for Marine-Earth Science and Technology, Kobe, Japan
[3]Observations Department, Japan Meteorological Agency, Otemachi, Japan
[4]Atmosphere and Ocean Research Institute, The University of Tokyo, Kashiwa, Japan

1. INTRODUCTION

Most of strong tornadoes are spawned by supercells (Browning 1964), which develop in an environment with strong vertical wind shear and unstable stratification, and are accompanied with mesocyclones. There have been a number of observational and numerical studies that attempted to clarify the mechanism of the tornadogenesis and the origin of the rotation of tornadoes. Recently, several deterministic high-resolution simulations having a horizontal grid interval of 100 m or less succeeded to reproduce geneses of observed tornadoes, and analyzed the origins of vorticity or circulation of the tornadoes. They suggest that either of horizontal vorticity associated with vertically-sheared environmental wind (Mashiko, 2009), baroclinically (Markowski et al. 2002, 2003, 2008; Straka et al. 2007; Mashiko, 2016a, b) or frictionally (Schenkman, 2012, 2014) generated horizontal vorticity or circulation is important for the tornadogenesis. However, which plays in general the most important role in providing the source of the rotation of tornadoes have not been clarified yet.

In order to deepen our understanding on the genesis mechanism of strong tornadoes and develop a possible technique for their forecast, statistical analyses using ensemble numerical experiments of observed tornadoes may be promising. Seko et al. (2015) and Yokota et al. (2016) have made ensemble simulations of the Tsukuba city (50–90 km northeast of Tokyo) F3 tornado on 6 May 2012, which is one of the strongest tornadoes observed in Japan. Horizontal resolution of their numerical model was 350 m, and the local ensemble transform Kalman filter (LETKF; Hunt et al. 2007) analysis was used as the initial conditions. Yokota et al. (2016) made an ensemble-based sensitivity analysis and showed that low-level convergence in the front side of the storm and low-level water vapor in the rear side of the storm controlled the strength of the forecasted low-level mesocyclone (LMC). However, the horizontal resolution used in Seko et al. (2015) and Yokota et al. (2016) was too coarse to examine the relationship between the strength of LMCs and the tornadogenesis.

In this study, we conducted ensemble forecasts for the Tsukuba city supercell tornado on 6 May 2012 with 50-m horizontal resolution and attempt to clarify the origin of the rotation of the tornado and essential factors for the tornadogenesis.

2. DATA ASSIMILATION WITH THE NESTED LETKF SYSTEM

The nested LETKF system (Seko et al. 2013) was used to assimilate dense observations around the tornado. In this system, Japan Meteorological Agency non-hydrostatic model (JMANHM; Saito et al. 2007) was used for the ensemble forecasts. Conventional observations, four C-band radars, and dense surface observations were assimilated with 4D-LETKF (Hunt et al. 2004, 2007) for models with 15-km and 1.875-km horizontal resolutions, respectively. 33-member downscale ensemble forecasts with 350-m horizontal resolution were performed from 1.875-km LETKF analysis at 1100JST (JST = UTC + 0900) as in Yokota et al. (2016).

In the present study, we additionally carried out 33-member downscale ensemble forecasts with 50-m horizontal resolution. In this downscale ensemble forecasts, the 33-member ensemble forecasts with 350-m horizontal resolution from 1110 to 1210JST were used as the initial and boundary conditions. The number of vertical levels was 90, and the vertical grid interval varied vertically from 10 m near the surface to 445 m near the top of the calculation domain. A first-order turbulence closure scheme based on Deardorff (1980) was adopted, and no cumulus parameterization was used. Figure 1 shows the outline of the experiments of this study.

3. FORECASTED TORNADO

The downscale ensemble forecasts with 50-m horizontal resolution produced a variety of tornado-scale vortices: some members resulted in strong vortices (maximum vertical vorticity at 30-m height $\zeta > 1\ \mathrm{s}^{-1}$), and some caused weaker vortices. The forecasted strong vortices were located on a linear region with steep near-surface temperature gradient (Fig. 2). The results of the downscale ensemble forecasts are used to clarify the relationship between the LMC and the tornado.

In the following, "tornado strength" ζ_{MAX} is defined by 5-minites averaged ζ. For a member having the largest ζ_{MAX}, vortex lines near the point of ζ erect nearly vertically at the time of maximum ζ (Fig. 3a). When ζ exceeded 0.6 s^{-1}, however, the vortex lines were arch-shaped above 30-m height and parallel to the sur-

---

* *Corresponding author address:* Sho Yokota, Meteorological Research Institute, 1-1, Nagamine, Tsukuba, Ibaraki, 305-0052, Japan; e-mail: syokota@mri-jma.go.jp

face below 30-m height (Fig. 3b). The arch-shaped vortex lines imply that the tornado was baroclinically generated (Markowski et al. 2002, 2003, 2008; Straka et al. 2007), while the vortex lines parallel to the surface imply that it was frictionally generated (Schenkman et al. 2012, 2014).

4．ORIGIN OF TORNADO CIRCULATION

To clarify the origin of the rotation of the tornado, we conducted circulation analyses for members having five strongest ζ_{MAX}. Circulation, which is a curvilinear integral of velocity $\boldsymbol{v}$ along a circuit, is generated only by baroclinity and friction as

$$\underbrace{\frac{D}{Dt}\oint \mathbf{v}\cdot d\mathbf{l}}_{\text{Circulation}} = \underbrace{-\oint \frac{dp}{\rho}}_{\text{Baroclinic term}} \underbrace{+\oint \mathbf{F}\cdot d\mathbf{l}}_{\text{Friction term}}, \qquad (1)$$

where ρ, p, and $\mathbf{F}$ are density, pressure, and frictional effect due to sub-grid turbulence, respectively. We calculated the circulation and the baroclinic and friction terms in Eq. (1) on the circuit backtracked from a circle of 100-m radius around the point of ζ when it exceeded 0.6 s^{-1} (Fig. 4). Backward trajectory of the circuit was calculated using the fourth-order Runge-Kutta scheme with an integration step of 1.0 s.

Figure 5 shows time series of the circulation and the baroclinic and friction terms for the five members. The friction term turned out to be larger than the baroclinic term in all five members, indicating that friction is the dominant contributor to change the circulation.

When the friction term was large, the circuit has a considerable vertical projection and the friction term per unit length was especially large near the surface (not shown). Although friction can increase the circulation of this circuit, it does not always do so in some members (for example, Figs. 5b and 5e). Moreover, features of time series of the baroclinic and friction terms seem to be unrelated to ζ_{MAX} (Fig. 5). Therefore, tornado strength does not seem to be determined by the generation terms of circulation.

5．CORRELATION OF TORNADO STRENGTH

If the origin of circulation is not essential for determining whether the vortices develop into tornadoes or not, stretching of vorticity due to shortening of the circuit is likely to be more important for a tornadogenesis. To clarify essential factors for the tornadogenesis, we produced composite fields with the coordinate system relative to the point and time of ζ_{MAX}, and calculated correlations of ζ_{MAX} to several variables in this composite field for the 33 members.

Correlation of ζ_{MAX} to mesocyclone-scale maximum vertical vorticity ζ_{MC}, calculated with 350-m horizontal resolution, was positive and especially large at about 1-km height right before the tornadogenesis (Fig. 6a). And ζ_{MC} at 1-km height for the members that spawned tornadic vortices ($\zeta_{\mathrm{MAX}} > 1\ s^{-1}$) was very close to the near-surface vortex. These results demonstrate that the stronger LMC at about 1-km height has more potential for a tornadogenesis. In fact, maximum updraft at 1-km height and vertical pressure gradient below 1-km height, which were related to LMCs, were also strongly correlated to ζ_{MAX} (not shown).

Figures 6b and 6c are correlations of ζ_{MAX} to water vapor and potential temperature averaged in the 30x30 km rectangular region around the point of ζ (hereafter, $\mathrm{QV_{MEAN}}$ and $\mathrm{PT_{MEAN}}$, respectively). The correlation to $\mathrm{QV_{MEAN}}$ was always positive. Right before the tornadogenesis, however, it is large only below 100-m height. Correlation to $\mathrm{PT_{MEAN}}$ was small and not significant at any height below 4 km.

At 3-minutes before the time of maximum ζ, ζ_{MC} at 1-km height and $\mathrm{QV_{MEAN}}$ averaged below 100-m height were more than 0.077 s^{-1} and 10.6 g kg^{-1} in the members that spawned tornadic vortices ($\zeta_{\mathrm{MAX}} > 1\ s^{-1}$). Correlation coefficients of ζ_{MAX} to these two factors were large (0.71 and 0.49, respectively). However, each of ζ_{MC} and $\mathrm{QV_{MEAN}}$, alone does not give an appropriate criteria for the tornadogenesis. To more accurately determine whether tornadoes are generated or not, both ζ_{MC} at 1-km height and $\mathrm{QV_{MEAN}}$ averaged below 100-m height need to be used. Figure 7 shows that both strong mesocyclone at 1-km height and large mixing ratio of water vapor below 100-m height are necessary for the tornadogenesis.

6．DISCUSSION

Importance of a strong LMC at 1-km height for the tornadogenesis is explained in terms of dynamic vertical perturbation pressure gradient force (VPPGF). Pressure perturbation under Boussinesq approximation is given as

$$p' = p'_d + p'_b\,, \qquad (2)$$

$$p'_d \propto -\frac{1}{\rho_0}\nabla^2 p'_d = \left(\frac{\partial u}{\partial x}\right)^2 + \left(\frac{\partial v}{\partial y}\right)^2 + \left(\frac{\partial w}{\partial z}\right)^2 + 2\left(\frac{\partial v}{\partial x}\frac{\partial u}{\partial y} + \frac{\partial w}{\partial x}\frac{\partial u}{\partial z} + \frac{\partial w}{\partial y}\frac{\partial v}{\partial z}\right), \qquad (3)$$

$$p'_b \propto -\frac{1}{\rho_0}\nabla^2 p'_b = -\frac{\partial B}{\partial z}, \qquad (4)$$

where p'_d is dynamic perturbation pressure and p'_b is perturbation pressure due to buoyancy B. Since the horizontal scale is small, Coriolis force is neglected. If an LMC is dominant over fluid extension, deformation, and horizontal vorticity, $p'_d \propto -\zeta^2/2$ is obtained from Eq. (3) near the LMC. Since p'_d is negative, upward acceleration due to dynamic VPPGF causes strong updraft at low-levels below the LMC, which in turn stretches vertical vorticity and contributes to the tornadogenesis.

Large water vapor below 100-m height also contributes to the upward acceleration by lowering lifted condensation level (LCL) and level of free convection (LFC): convection is more easily driven due to stronger positive buoyancy above LFC and weaker negative buoyancy above LCL. VPPGF derived by p'_b also enhances updraft below LCL because vertical gradient of B in Eq. (4) is large at LCL.

Buoyancy near the surface is also expected to be increased by higher virtual potential temperature due to larger water vapor and possibly associated suppression of evaporation cooling. The small correlation between ζ_{MAX} and $\mathrm{PT_{MEAN}}$, however, suggests that the latter hardly affect the tornadogenesis.

The above discussion may be summarized as follows: There may not be a universal origin of rotation in tornadoes, but could be any circulation. The most important factors for the tornadogenesis are (i) large dynamic VPPGF associated with a strong LMC and (ii) large buoyancy and buoyancy VPPGF due to low-level humid air, which causes strong low-level updraft that stretches existing low-level vertical vorticity.

7 . SUMMARY

In this study, we performed ensemble forecasts for the Tsukuba city supercell tornado on 6 May 2012 with 50-m horizontal resolution through assimilation of four radars' data and dense surface data with LETKF. We analyzed the origin of the tornado circulation through a backward trajectory analysis, and clarified factors important for the tornadogenesis by examining correlations of tornado strength with physical variables.

The results of the trajectory analysis showed that friction played dominant role in the change of the circulation that went into the tornado vortex. However, friction can have either positive or negative sign and the tornado strength had little correlation to the changes of the circulation by friction. On the other hand, it was confirmed that a strong LMC at about 1-km height and near-surface humid air were important factors for the tornadogenesis. They cause larger upward accelerations through VPPGF and buoyancy and are highly correlated to the strength of the tornado vortex. These results show that low-level convergence and water vapor, which were also noted as significant factors in Yokota et al. (2016), are important factors for both strength of LMCs and the tornadogenesis.

ACKNOWLEDGEMENTS

This work was supported in part by the research project ''HPCI Strategic Program for Innovative Research (SPIRE) Field 3,'' ''Social and Scientific Priority Issues (Theme 4) to Be Tackled by Using Post K Computer of the FLAGSHIP2020 Project,'' ''Tokyo Metropolitan Area Convection Study for Extreme Weather Resilient Cities (TOMACS),'' JSPS Kakenhi No. 24244074, and the Cooperative Program (No. 131, 2014; No. 136, 2015; No. 138, 2016) of Atmosphere and Ocean Research Institute, The University of Tokyo. Experiment with 350-m and 50-m horizontal resolution were conducted using the K computer at the RIKEN Advanced Institute for Computational Science through the HPCI System Research Project (Project ID: hp120282, hp130012, hp140220, hp150214, hp150289, hp160229). Observational data were provided from JMA and NTT DOCOMO, Inc.

REFERENCES

Browning, K. A., 1964: Airflow and precipitation trajectories within severe local storms which travel to the right of the winds. *J. Atmos. Sci.*, **21**, 634–639.

Deardorff, J. W., 1980: Stratocumulus-capped mixed layers derived from a three-dimensional Model. *Bound.-Layer Meteor.*, **18**, 495–527.

Hunt, B. R., and Coauthors, 2004: Four-dimensional ensemble Kalman filtering. *Tellus*, **56A**, 273−277.

Hunt, B. R., E. J. Kostelich, and I. Szunyogh, 2007: Efficient data assimilation for spatiotemporal chaos: A local ensemble transform Kalman filter. *Phys. D*, **230**, 112–126.

Markowski, P. M., and Y. P. Richardson, 2014: The influence of environmental low-level shear and cold pools on tornadogenesis: Insights from idealized simulations, *J. Atmos. Sci.*, **71**, 243-275.

Markowski, P. M., J. M. Straka, and E. N. Rasmussen, 2002: Direct surface thermodynamic observations within the rear-flank downdrafts of nontornadic and tornadic supercells. *Mon. Wea. Rev.*, **130**, 1692–1721.

Markowski, P. M., J. M. Straka, and E. N. Rasmussen, 2003: Tornadogenesis resulting from the transport of circulation by a downdraft: Idealized numerical simulations. *J. Atmos. Sci.*, **60**, 795–823.

Markowski, P. M., Y. P. Richardson, E. Rasmussen, J. Straka, R. Davies-Jones, and R. J. Trapp, 2008: Vortex lines within low-level mesocyclones obtained from pseudo-dual-Doppler radar observations. *Mon. Wea. Rev.*, **136**, 3513–3535.

Mashiko, W., 2016a: A numerical study of the 6 May 2012 Tsukuba city supercell tornado. Part I: Vorticity sources of low-level and midlevel mesocyclones. *Mon. Wea. Rev.*,**144**, 1069–1092.

Mashiko, W., 2016b: A numerical study of the 6 May 2012 Tsukuba City supercell tornado. Part II: Mechanisms of tornadogenesis., *Mon. Wea. Rev.*, **144**, 3077–3098.

Mashiko, W., H. Niino, and T. Kato, 2009: Numerical simulation of tornadogenesis in an outer-rainband minisupercell of typhoon Shanshan on 17 September 2006. *Mon. Wea. Rev.*, **137**, 4238–4260.

Rotunno, R., and J. B. Klemp, 1982: The influence of the shear-induced pressure gradient on thunderstorm motion. *Mon. Wea. Rev.*, **110**, 136–151.

Saito, K., and Coauthors, 2006: The operational JMA nonhydrostatic mesoscale model. *Mon. Wea. Rev.*, **134**, 1266–1298.

Schenkman, A. D., M. Xue, and A. Shapiro, 2012: Tornadogenesis in a simulated mesovortex within a mesoscale convective system, *J. Atmos. Sci.*, **69**, 3372–3390.

Schenkman, A. D., M. Xue, and M. Hu, 2014: Tornadogenesis in a high-resolution simulation of the 8 May 2003 Oklahoma City supercell., *J. Atmos. Sci.*, **71**, 130–154.

Seko, H., T. Tsuyuki, K. Saito, and T. Miyoshi, 2013: Development of a two-way nested LETKF system for cloud-resolving model. *Data Assimilation for Atmospheric, Oceanic and Hydrologic Applications*, **2**, 489–507.

Seko, H., M. Kunii, S. Yokota, T. Tsuyuki, and T. Miyoshi, 2015: Ensemble experiments using a nested LETKF system to reproduce intense vortices associated with tornadoes of 6 May 2012 in Japan. *Prog. Earth Planet. Sci.*, **2**, 42.

Straka, J. M., E. N. Rasmussen, R. P. Davies-Jones, and P. M. Markowski, 2007: An observational and idealized numerical examination of low-level counter-rotating vortices in the rear flank of supercells. *Electronic J. Severe Storms Meteor.*, **2**, 1–22

Yokota, S., H. Seko, M. Kunii, H, Yamauchi, and H. Niino, 2016: The tornadic supercell on the Kanto Plain on 6 May 2012: Polarimetric radar and surface data assimilation with EnKF and ensemble-based sensitivity analysis., *Mon. Wea. Rev.*, **144**, 3133–3157.

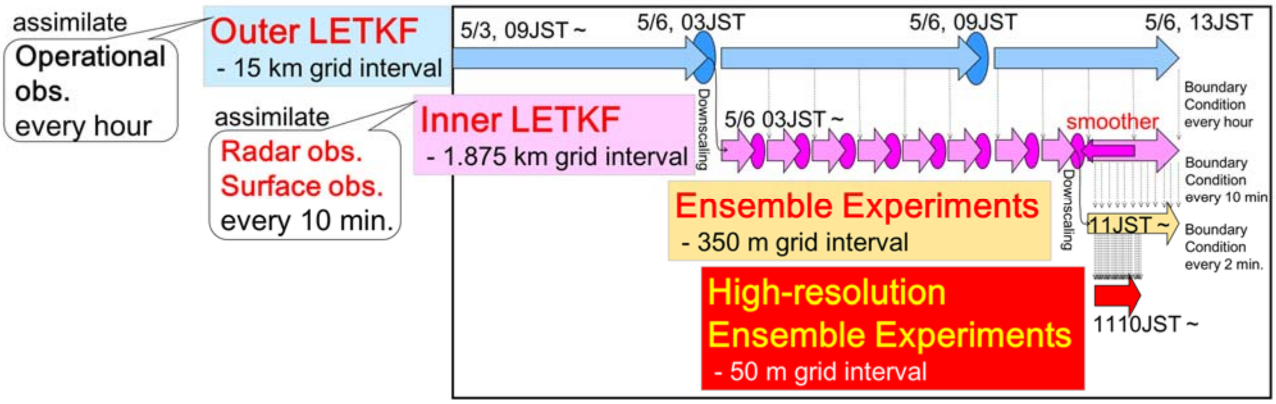

Fig. 1. Outline of the nested LETKF system and the ensemble forecasts used in this study.

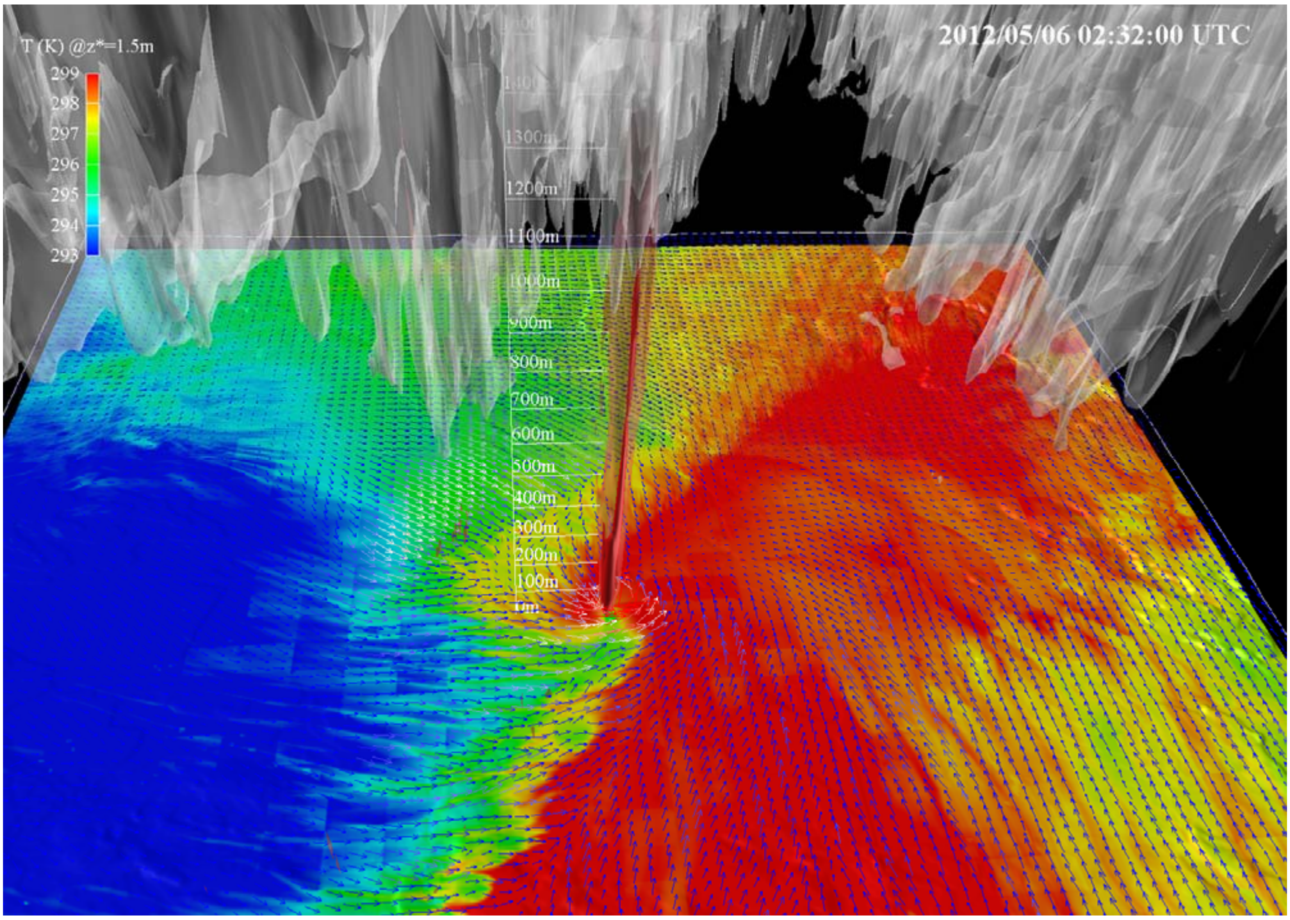

Fig. 2. The three-dimensional structure of the forecasted tornadic vortex at 1132JST in the member of strongest ζ_{MAX}. Red isosurfaces are 0.2-s^{-1} (translucent) and 0.6-s^{-1} (opaque) vertcal vorticity. White isosurfaces are 1-g kg^{-1} cloud water mixing ratio. Color is temperature at 1.5-m height (K). Arrows are horizontal wind at 30-m height (m s^{-1}), where blue, white, and red arrows show less than 20 m s^{-1}, between 20 and 40 m s^{-1}, more than 40 m s^{-1}, respectively.

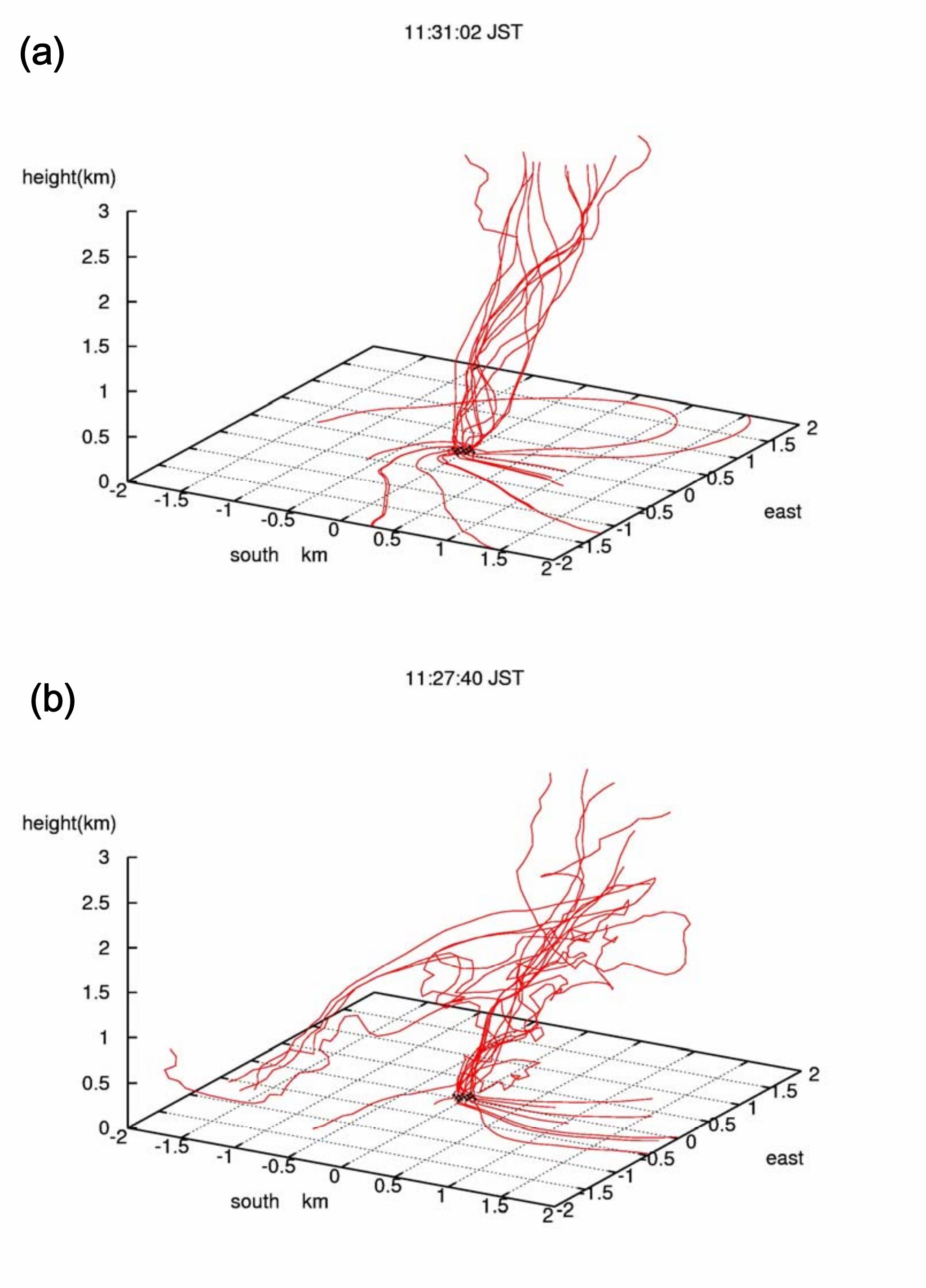

Fig. 3. Vortex lines through the circle of 100-m radius around ζ when ζ is (a) maximum and (b) exceeded 0.6 s^{-1} in the member of strongest ζ_{MAX}.

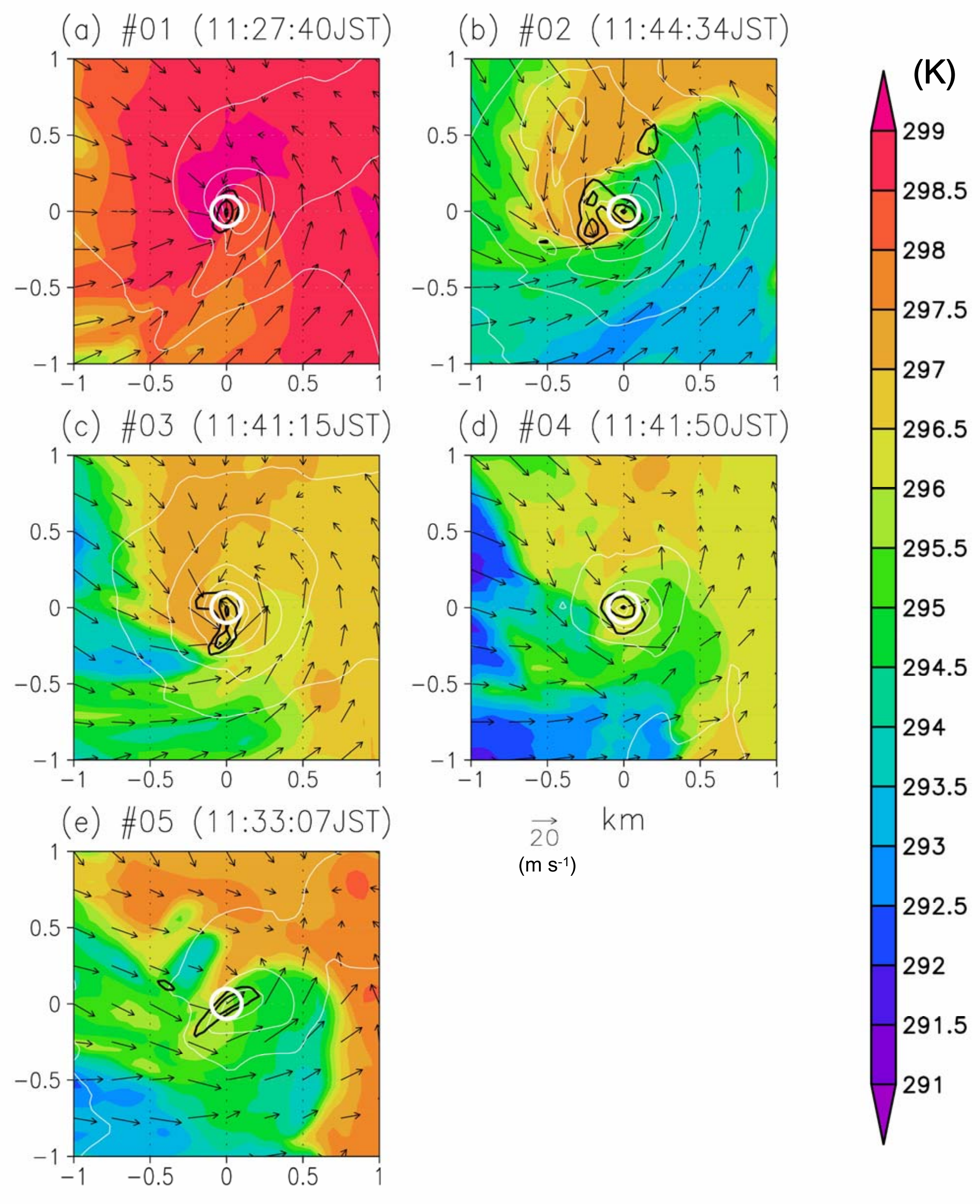

Fig. 4. Horizontal wind (arrows, m s^{-1}), potential temperature (color, K), pressure (thin white contour, every 2 hPa), and vertical vorticity (black contour, every 0.2 s^{-1}) when ζ exceeded 0.6 s^{-1} at 30-m height. (a)–(e) show the results of five members in order of stronger ζ_{MAX}. The centers of the figures are taken to the points of ζ. Thick white circles show the circuits where the circulations were analyzed in Fig. 5.

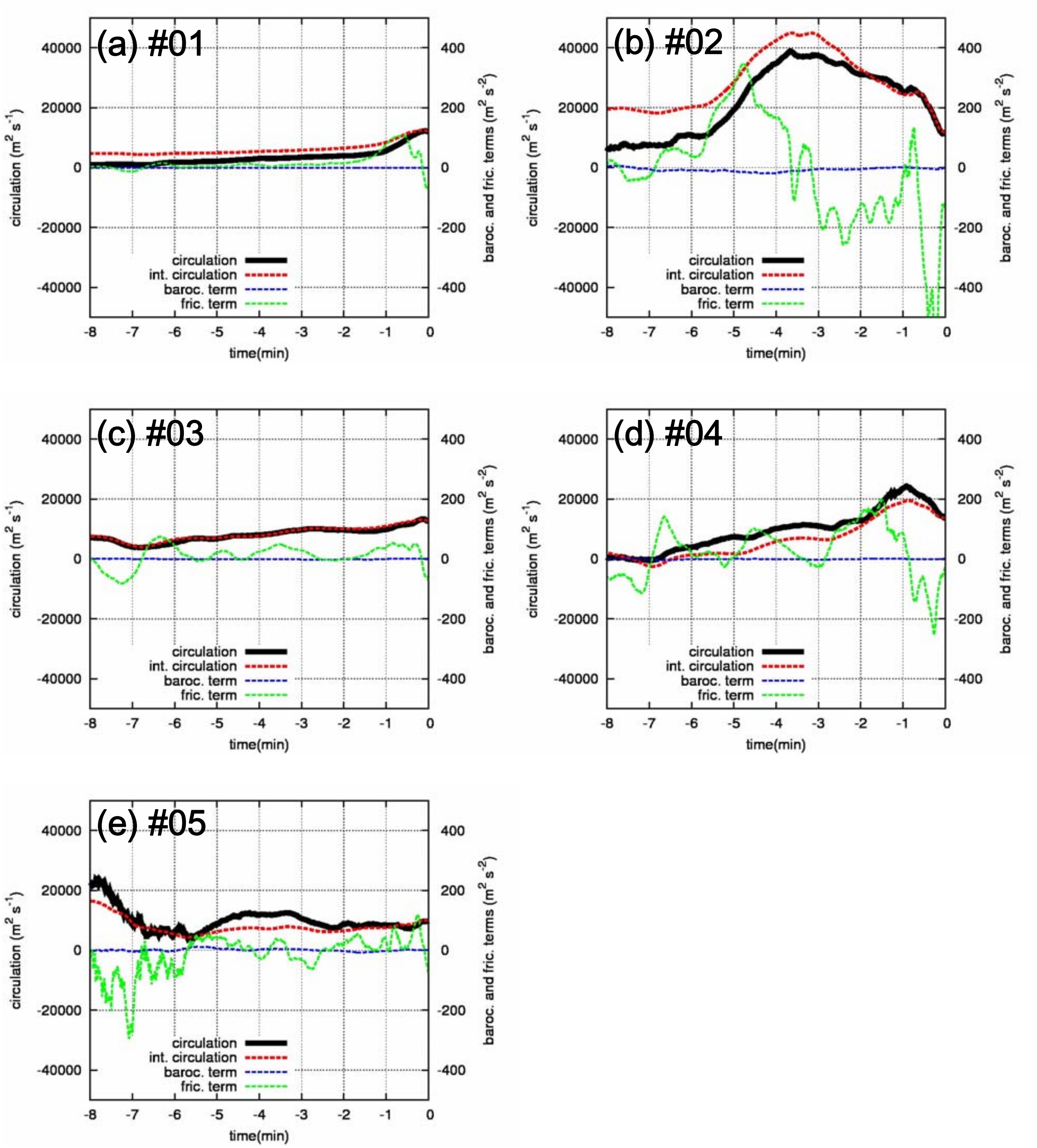

Fig. 5. Time series of the circulation (black) and the baroclinic (blue) and friction (green) terms calculated along the circuits backtracked from thick white circles shown in Fig. 4. (a)–(e) show the results of five members in order of stronger ζ_{MAX}. Red lines are the circulations calculated by integrating the baroclinic and friction terms.

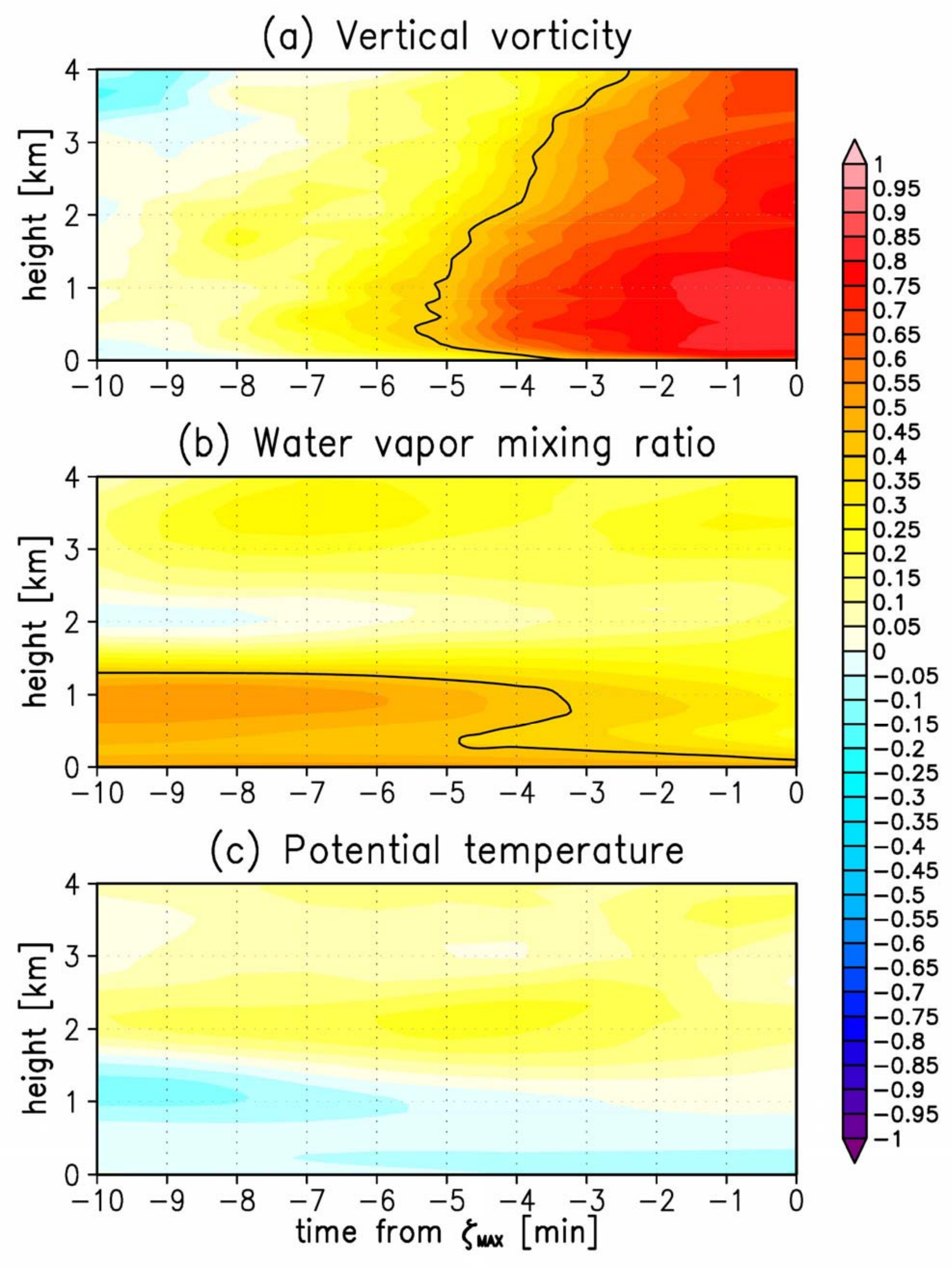

Fig. 6. Distribution of correlations of ζ_{MAX} (s^{-1}) to (a) ζ_{MC} (s^{-1}), (b) $\mathrm{QV}_{\mathrm{MEAN}}$ (g kg^{-1}), and (c) $\mathrm{PT}_{\mathrm{MEAN}}$ (K). Vertical axis is height (km), and horizontal axis is time from maximum ζ at 30-m height (minutes). Black lines are 0.4.

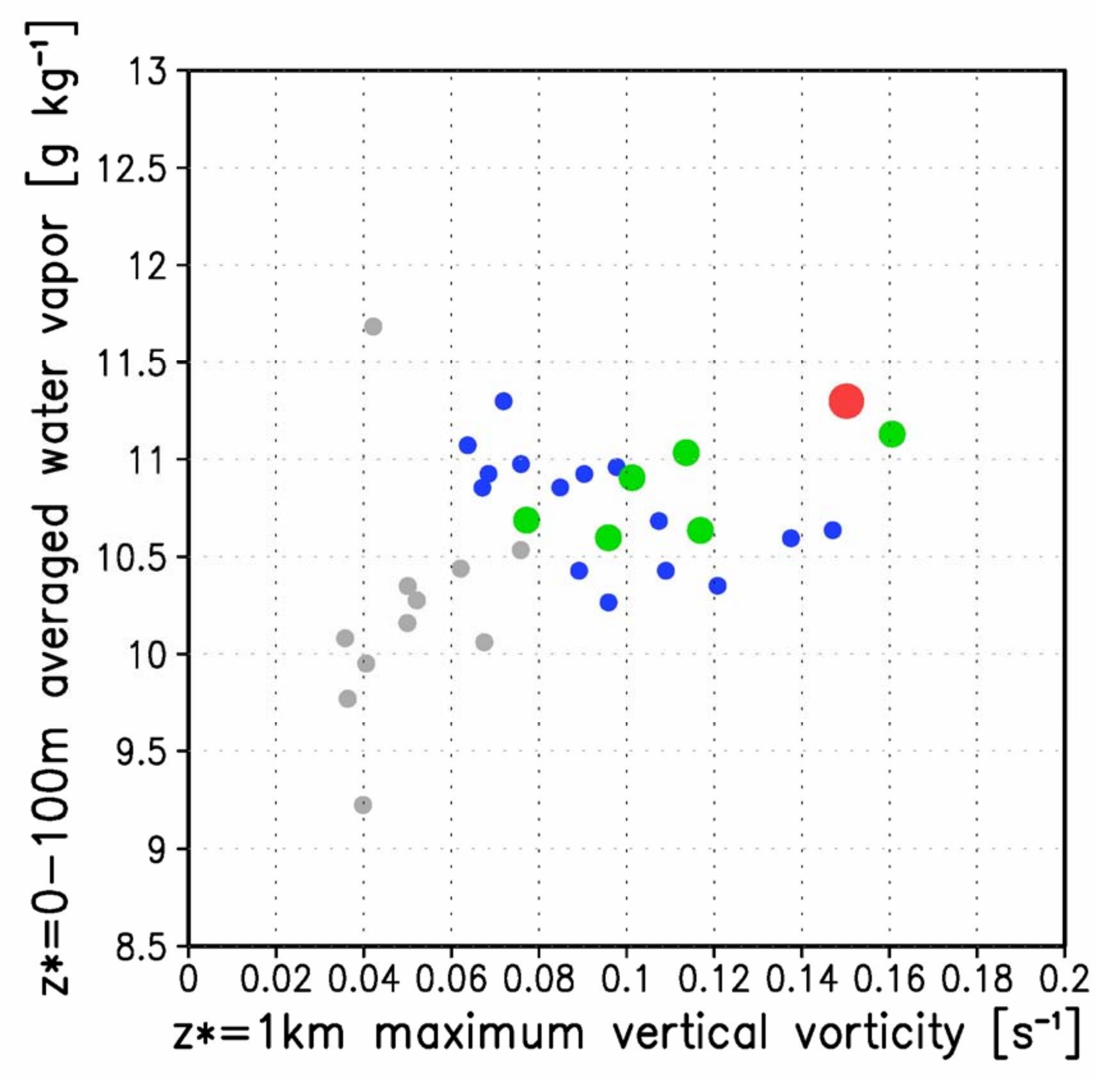

Fig. 7. Scatter plot of ζ_{MC} at 1-km height (s^{-1}) and $\mathrm{QV}_{\mathrm{MEAN}}$ averaged below 100-m height (g kg^{-1}) 3-minutes before the time of ζ_{MAX} in 33 ensemble members. Gray, blue, big green, and big red marks show that ζ_{MAX} is less than 0.7 s^{-1}, between 0.7 and 1.0 s^{-1}, more than 1.0 s^{-1}, and strongest, respectively.